

Journal Pre-proof

Simultaneous removal of ammonia and phosphate by electro-oxidation and electrocoagulation using RuO₂-IrO₂/Ti and microscale zero-valent iron composite electrode

Dongni Sun, Xiaoting Hong, Keming Wu, K.S. Hui, Yingying Du, K.N. Hui

PII: S0043-1354(19)31013-9

DOI: <https://doi.org/10.1016/j.watres.2019.115239>

Reference: WR 115239

To appear in: *Water Research*

Received Date: 16 July 2019

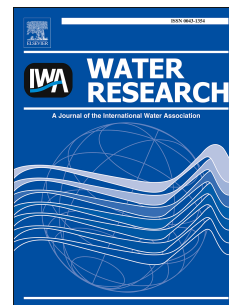
Revised Date: 21 October 2019

Accepted Date: 25 October 2019

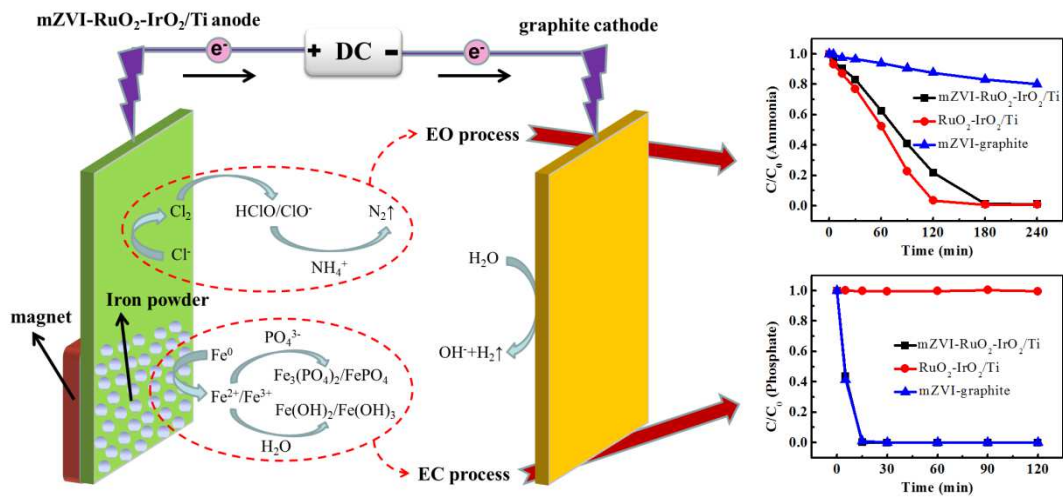
Please cite this article as: Sun, D., Hong, X., Wu, K., Hui, K.S., Du, Y., Hui, K.N., Simultaneous removal of ammonia and phosphate by electro-oxidation and electrocoagulation using RuO₂-IrO₂/Ti and microscale zero-valent iron composite electrode, *Water Research* (2019), doi: <https://doi.org/10.1016/j.watres.2019.115239>.

This is a PDF file of an article that has undergone enhancements after acceptance, such as the addition of a cover page and metadata, and formatting for readability, but it is not yet the definitive version of record. This version will undergo additional copyediting, typesetting and review before it is published in its final form, but we are providing this version to give early visibility of the article. Please note that, during the production process, errors may be discovered which could affect the content, and all legal disclaimers that apply to the journal pertain.

© 2019 Published by Elsevier Ltd.



Graphical abstract



24 **Abstract:** Electro-oxidation using RuO₂-IrO₂/Ti plate anode and electrocoagulation
25 using iron plate anode were widely applied to remove ammonia and phosphate in an
26 aquatic environment, respectively. In this work, we designed magnetically bound ZVI
27 microparticles on RuO₂-IrO₂/Ti plate as a composite electrode for the simultaneous
28 removal of ammonia and phosphate from aqueous solution via combined EO and EC
29 (EO/EC) processes. We present a series of experiments to study such simultaneous
30 removal under an electric field via the EO/EC process. In the electrochemical unit,
31 mZVI-RuO₂-IrO₂/Ti, mZVI-graphite, and RuO₂-IrO₂/Ti electrodes were used as
32 anodes. The influence of applied voltage, initial pH, zero-valent iron dosage, reaction
33 temperature, and organic compounds on the EO/EC process was also examined.
34 Ammonia and phosphate could be completely removed at an applied voltage of 10 V,
35 pH of 7, zero-valent iron dosage of 0.1 g, and reaction temperature of 35 °C using
36 mZVI-RuO₂-IrO₂/Ti anode when influent ammonia and phosphate concentrations is
37 200 and 100 mg·L⁻¹. Ammonia degradation was consistent with pseudo-zero-order
38 kinetic model. The characterization was analyzed by scanning electron
39 microscope-energy dispersive spectrometer (SEM-EDS), X-ray diffraction (XRD) and
40 X-ray photoelectron spectroscopy (XPS). Hence, the mZVI-RuO₂-IrO₂/Ti electrode
41 can be used for efficient simultaneous removal of ammonia and phosphate.

42

43 **Key words:** ammonia; phosphate; electro-oxidation; electrocoagulation; zero-valent
44 iron

45 **1. Introduction**

46 In recent years, eutrophication of freshwater and coastal marine ecosystems has
47 become an increasingly serious problem (Smith and Schindler 2009). In particular, the
48 large amounts of ammonia and phosphate emitted in municipal and industrial plants
49 were considered the main cause of eutrophication (Irdemez et al. 2006, Zhang et al.
50 2018a). Excessive amounts of nitrogen and phosphate in the water will stimulate the
51 blue-green algae to multiply under appropriate temperature conditions and consume a
52 large amount of dissolved oxygen, leading to the death of aquatic organisms (Su et al.
53 2013).

54 Many technologies are used for ammonia and phosphate wastewater treatment such
55 as nitrification and denitrification (Jih et al. 2001, Ruiz et al. 2006), anaerobic
56 ammonium oxidation (Laureni et al. 2016), breakpoint chlorination (Pressley et al.
57 1972), ammonia-stripping (Bonmati and Flotats 2003), adsorption (Boujelben et al.
58 2008, Huang et al. 2010), ion exchange (Bashir et al. 2010, Choi et al. 2011),
59 microwave radiation (Lin et al. 2009), chemical precipitation (Jaffer et al. 2002), and
60 capacitive deionization methods (Ma et al. 2018). The methods for simultaneously
61 removing nitrogen and phosphate are mainly biodegradation and adsorption. Bassin et
62 al. investigated laboratory-scale sequencing batch reactors that were operated at
63 different temperatures (20 and 30 °C) for aerobic granular sludges, and simultaneous
64 nitrogen and phosphate removal was achieved (Bassin et al. 2012). Huang et al. found
65 that natural zeolite can be modified by magnesium salts and used as an adsorbent

66 material to simultaneously remove ammonia and phosphate from simulated swine
67 wastewater (Huang et al. 2014). Yin et al. investigated the use of natural calcium-rich
68 attapulgite to develop a versatile adsorbent that can simultaneously remove ammonia
69 and phosphate from contaminated waters (Yin and Kong 2014).

70 In recent years, electrochemical technology has been increasingly used to treat
71 wastewater containing ammonia and phosphate due to its short reaction process, small
72 footprint, easy operation, and high removal efficiency. Among these electrochemical
73 technologies, the most studied are electro-oxidation (EO) and electrocoagulation (EC)
74 for ammonia and phosphate wastewater, respectively.

75 EO is an advanced oxidation process that efficiently converts ammonia into
76 harmless nitrogen gas by either direct or indirect oxidation (Li and Liu 2009). Direct
77 EO involves ammonia adsorption onto the anode surface, its direct electron transfer,
78 and ultimately, its conversion into nitrogen gas (Kapałka et al. 2010a). Conversely,
79 indirect EO of ammonia is performed via anodic reaction to form an intermediate
80 oxidant (e.g., Cl_2 , HClO , and ClO^-), which is then reacted with ammonia for
81 ammonia removal (Kapałka et al. 2010b). Considerable investigations have been
82 conducted on different anode materials for EO. Ammonia was removed thoroughly
83 when boron-doped diamond anode was used for the treatment of cooking wastewater
84 (Zhu et al. 2009). Furthermore, ammonia was almost completely removed when metal
85 oxide electrodes (Ti/PbO_2 and Ti/SnO_2 anodes) were used for the treatment of landfill
86 leachate (Cossu et al. 1998). Dimensional stability anode containing Ru, Ir, or Ti has

87 been widely used in wastewater treatment due to its good electrocatalytic performance,
88 greater stability, long service life, low price and higher availability (Costa et al. 2008,
89 Li et al. 2013, Profeti et al. 2006). Ihara et al. found that RuO₂-IrO₂/Ti was a more
90 suitable anode for decreasing ammonia and controlling nitrate accumulation than
91 Ti/PbO₂ (Ihara et al. 2006).

92 Meanwhile, EC has been widely used in wastewater treatment because of its high
93 efficiency and simple operation (Fernandes et al. 2015, Heidmann and Calmano 2008).
94 Chemical coagulation requires a large amount of coagulant, but EC overcomes this
95 problem by directly generating coagulants via anodic dissolution (Zhang et al. 2018b).
96 In EC, coagulants are generated in situ via electrically dissolving metal ions, such as
97 Fe²⁺/Fe³⁺ and Al³⁺, from metal electrodes. The generated Fe²⁺/Fe³⁺ or Al³⁺ ions are
98 effective coagulants for particle flocculation (Chen 2004). Iron and aluminum plates
99 are the most commonly used electrodes for phosphate removal; specifically,
100 aluminum plate exhibits high and stable removal efficiency (Bektas et al. 2004).
101 Zheng et al. evaluated the effects of various experimental parameters, including
102 current density, gap between electrodes, urine dosage, dilution, and hydrolysis, on
103 phosphate removal from urine via EC using iron as anode (Zheng et al. 2009).

104 Previous studies have suggested the potential of RuO₂-IrO₂/Ti plate as an anode for
105 ammonia removal through EO and iron plate as an anode for phosphate removal
106 through EC. However, the use of pure RuO₂-IrO₂/Ti anode can only remove ammonia
107 and cannot remove phosphate because the latter cannot be oxidized. On the contrary,

108 the use of pure iron anode can only remove phosphate and is less effective in
 109 removing ammonia because it is prone to oxygen evolution side reaction. To achieve
 110 the purpose of simultaneous ammonia and phosphate removal, we designed a
 111 zero-valent iron powder and RuO₂-IrO₂/Ti plat composite electrode
 112 (mZVI-RuO₂-IrO₂/Ti). Iron powder was bound to the RuO₂-IrO₂/Ti plat by a magnetic
 113 field. This system has both oxidation and coagulation compared to a single EO and a
 114 single EC system. In addition, this system is simple in operation, high in efficiency,
 115 and short in reaction time compared to the biological method.

116 The reaction in the electrode and in the aqueous solution is as follows (Gendel and
 117 Lahav 2012, Omwene et al. 2018, Tian et al. 2018):

118 Anode:



121 Aqueous phase:



129 Cathode:



131 The present study examines the combined EO and EC (EO/EC) processes for
132 ammonia and phosphate removal in aqueous solution. The evaluated parameters were
133 anode materials, applied voltage, and initial pH. The effects of zero-valent iron dosage,
134 reaction temperature and organic compounds were also evaluated. The characteristics
135 of the precipitation were investigated via scanning electron microscopy–energy
136 dispersive spectrometry, X-ray diffraction (XRD), and X-ray photoelectron
137 spectroscopy (XPS). This study is the first to investigate and propose the possible
138 mechanism of the simultaneous removal of ammonia and phosphate under an electric
139 field in a magnetically bound zero-valent iron powder and RuO₂-IrO₂/Ti composite
140 anode by combining EO and EC processes.

141

142 **2. Materials and methods**

143 **2.1 Chemical reagents and synthetic solution**

144 The synthetic solution was obtained by dissolving (NH₄)₂SO₄, KH₂PO₄, and NaCl
145 in ultrapure water with resistivity of 18.2 MΩ-cm from the Milli-Q (Millipore) water
146 purification system. The synthetic solution contains 200, 100, and 500 mg·L⁻¹ of N, P,
147 and Cl⁻. The influent ammonia and phosphate concentrations were close to some
148 aquaculture wastewater that we had encountered. The pH of aqueous solution was
149 adjusted by adding 3 M of NaOH or 1 M of H₂SO₄ according to the requirements of

150 the experimental design. The conductivity of aqueous solution was adjusted to 750 μS
151 cm^{-1} by adding 1 M of Na_2SO_4 . All reagents were obtained from Aladdin Chemistry
152 Co., Ltd. (Shanghai, China). They were of analytical grade and used without further
153 refinement. Furthermore, microscale zero-valent iron powder (>98%) was purchased
154 from Tianjin Shentai Chemical Reagent Co., Ltd. $\text{RuO}_2\text{-IrO}_2/\text{Ti}$ plate and graphite
155 flakes were supplied by Hebei Mingxuan Metal Materials Co., Ltd. and Qingdao
156 Baofeng Graphite Co., Ltd., respectively. The surface of the titanium plate is an oxide
157 coating of Ru and Ir, the mass ratio of Ru to Ir is about 7:3.

158

159 **2.2 Experimental setup**

160 All batch mode experiments were conducted in a 200 mL electrolyte glass tank and
161 maintained at a constant temperature (25, 35, 45, and 55 °C) by heating in a water
162 bath. The area of the $\text{RuO}_2\text{-IrO}_2/\text{Ti}$ plate immersed in the solution was 15 cm^2 . A
163 certain amount of mZVI powder was evenly distributed on a $\text{RuO}_2\text{-IrO}_2/\text{Ti}$ plate with
164 a size of $2.5 \times 10 \text{ cm}^2$ and a thickness of 0.1 cm, and the mZVI powder occupied an
165 area of 8 cm^2 (2 cm \times 4 cm). The mZVI powder was fixed on the surface of the
166 $\text{RuO}_2\text{-IrO}_2/\text{Ti}$ plate through a 4 cm \times 2 cm \times 0.5 cm magnet (surface magnetic field
167 strength \sim 2004 gauss) outside the glass reactor as mZVI- $\text{RuO}_2\text{-IrO}_2/\text{Ti}$ composite
168 anode. An mZVI-graphite composite anode was also prepared by replacing the
169 $\text{RuO}_2\text{-IrO}_2/\text{Ti}$ plate with a graphite sheet. The mZVI- $\text{RuO}_2\text{-IrO}_2/\text{Ti}$ anode and graphite
170 cathode were placed in parallel, and the gap between them was maintained at 1 cm.

171 The electrodes were connected to a DC power source to assemble the EO/EC reactor.

172 The experimental setup is shown in Fig. 1.

173

174 **2.3 Experimental methods**

175 Numerous factors influencing ammonia and phosphate removal in the EO/EC
176 process were investigated. These factors include anode materials, applied voltage,
177 initial pH, zero-valent iron dosage, reaction temperature, and organic compounds. The
178 mZVI-RuO₂-IrO₂/Ti, mZVI-graphite, and RuO₂-IrO₂/Ti electrodes were used as the
179 anodes in our experiments. Given that the iron powder was bound to the electrode, the
180 effective area of the electrode cannot be accurately calculated, and obtaining the
181 current density was difficult; hence, we used constant voltage (ranging from 4 V to 10
182 V) from DC power supply. The initial pH (3 to 11) of the solution was adjusted by
183 adding 1 M of H₂SO₄ or 3 M of NaOH. The amount of iron powder was also
184 investigated as a factor influencing the efficiency of phosphate removal. The
185 experiment was performed at different temperatures (25, 35, 45, and 55 °C).

186 Each set of experiments was performed for 4 h to 6 h, and samples of the solution
187 were collected at designated times during the experiment. Before analysis, each
188 sample was filtered through membrane filters with 0.45 μm pore diameter. Ammonia,
189 nitrate, nitrite and phosphate were determined with a continuous flowing analyzer
190 (Seal AA3, Germany). After the reaction, the total soluble iron ion concentration in
191 the solution was measured by inductively coupled plasma emission spectroscopy. The

192 Cl^- concentration was determined using standard methods, such as silver nitrate
 193 titration method. The conductivity and pH of the solution were determined using
 194 conductivity (Rex Chemical Corp., Shanghai) and pH meters (SevenMulti,
 195 Mettler-Toledo International Inc.).

196 The removal rate based on initial and final concentrations was calculated. It can be
 197 expressed as follows (Bashir et al. 2010):

$$198 \quad \eta = \frac{C_0 - C_t}{C_0} \times 100\% \quad (11)$$

199 where η is the ammonia and phosphate removal rate, C_0 is the initial concentration
 200 ($\text{mg}\cdot\text{L}^{-1}$) of ammonia or phosphate, and C_t is the final concentration ($\text{mg}\cdot\text{L}^{-1}$) of
 201 ammonia or phosphate.

202 Energy consumption is generally used to evaluate the performance of an
 203 electrochemical technology. It can be expressed as follows (Xue et al. 2020):

$$204 \quad \text{Energy consumption} = \frac{UIt}{(C_0 - C_t) \times V} \quad (12)$$

205 where U is the voltage applied (V), I is the current intensity (A), t is the EO/EC
 206 process time (h), and V represents the volume of the electrolyte (0.2 L).

207

208 **2.4 Characterization techniques**

209 The precipitate was collected after the reaction and then vacuum-dried. The
 210 partially dried precipitate was calcined at $600\text{ }^\circ\text{C}$ for 2 h under nitrogen atmosphere.
 211 XRD patterns before and after calcination were recorded using the PANalytical X'Pert
 212 PRO (Netherlands) diffractometer with monochromatic $\text{Cu K}\alpha$ irradiation in the 2 θ

213 angular regions between 5° and 80° . The surface morphologies and atomic
214 composition, as well as distribution, of the precipitate were determined by scanning
215 electron microscope (SEM, Phenom ProX, Phenom-World, Netherlands). XPS
216 measurements were performed on the Thermo Fisher Scientific ESCALAB 250Xi
217 XPS spectrometer (USA) using Al K α radiation with photon energy of 1486.6 eV as
218 the radiation source.

219

220 **3. Results and discussion**

221 *3.1 Influencing factors of the EO/EC process*

222 *3.1.1 Anode materials*

223 Anode materials play an important role in the EO/EC process. To investigate the
224 role of anode materials in ammonia and phosphate removal, we compared the EO/EC
225 performance of mZVI-RuO₂-IrO₂/Ti, mZVI-graphite, and RuO₂-IrO₂/Ti anodes. SEM
226 image of zero-valent iron powder is shown in Fig. S1. As can be seen, zero-valent iron
227 powder agglomeration is evident. The agglomerated iron powder was found to have a
228 particle size of less than 100 μm , which confirmed that the iron powder we used was
229 micron-sized. The mZVI-RuO₂-IrO₂/Ti and RuO₂-IrO₂/Ti anodes were considerably
230 better than the mZVI-graphite anode for ammonia removal (Fig. 2a). The
231 mZVI-graphite anode only removed 19.87% of the ammonia after 4 h of electrolysis.
232 This finding can be attributed to the fact that the RuO₂-IrO₂/Ti anode has a higher
233 oxygen evolution potential than the graphite electrode (Fan et al. 2013), resulting in a

234 large amount of oxygen on the mZVI-graphite anode surface but with slight
235 intermediate oxidation (Cl_2). Although $\text{RuO}_2\text{-IrO}_2/\text{Ti}$ and $\text{mZVI-RuO}_2\text{-IrO}_2/\text{Ti}$ anodes
236 both could completely remove the ammonia, the former anode removed ammonia at a
237 slightly faster rate than the latter (120 and 180 min for $\text{RuO}_2\text{-IrO}_2/\text{Ti}$ anode and
238 $\text{mZVI-RuO}_2\text{-IrO}_2/\text{Ti}$ anode, respectively). Hence, on the surface of $\text{RuO}_2\text{-IrO}_2/\text{Ti}$
239 anode, only Cl^- lost electrons, whereas on the surface of $\text{mZVI-RuO}_2\text{-IrO}_2/\text{Ti}$ anode,
240 in addition to the loss of electrons from Cl^- , electron transfer in iron powder occurred.

241 However, the pure $\text{RuO}_2\text{-IrO}_2/\text{Ti}$ anode has no effect on phosphate removal (Fig.
242 2d). This is mainly due to that the dissolved Fe^{2+} forms a precipitate with the
243 phosphate in the solution. With dissolved oxygen, Fe^{2+} was oxidized to Fe^{3+} , and Fe^{3+}
244 also reacted with phosphate to form a precipitate. Compared with that of the
245 $\text{mZVI-RuO}_2\text{-IrO}_2/\text{Ti}$ anode during the EO/EC process, the surface of the
246 $\text{RuO}_2\text{-IrO}_2/\text{Ti}$ anode had no iron powder; hence, only EO process occurred when
247 $\text{RuO}_2\text{-IrO}_2/\text{Ti}$ plate was used as the anode. This phenomenon confirmed the feasibility
248 of using $\text{mZVI-RuO}_2\text{-IrO}_2/\text{Ti}$ anode for the simultaneous removal of ammonia and
249 phosphate.

250 In the EO/EC process using $\text{mZVI-RuO}_2\text{-IrO}_2/\text{Ti}$ anode, the Cl^- and NH_4^+
251 concentrations in the solution consistently demonstrated the same decreasing trend
252 during the first 180 min of reaction time (Fig. 3a). A cycle of
253 chloride–chlorine–hypochlorite–chloride occurred in the EO process (Chen et al.
254 2007). When NH_4^+ was almost completely removed, Cl^- concentration decreased

255 rapidly. This result may be due to the fact that the HClO produced did not react with
256 more NH_4^+ , resulting in the interruption of the
257 chloride–chlorine–hypochlorite–chloride cycle. In addition, no nitrite was formed in
258 the solution, but nitrate and total soluble iron ions, which were lower than 3 and 2
259 $\text{mg}\cdot\text{L}^{-1}$, respectively, in the solution slightly accumulated. When the reaction
260 proceeded to 5 min, the total iron content in the solution increased ($1.89 \text{ mg}\cdot\text{L}^{-1}$), but
261 after the 30 min reaction, no iron ions were detected in the solution. At the same time,
262 the phosphate was completely removed within 30 min, and after 30 min, the iron ion
263 concentration in the solution gradually increased to finally reach $2.00 \text{ mg}\cdot\text{L}^{-1}$. This
264 occurrence may be due to the fact that the solution gradually becomes acidic as the
265 reaction proceeds, and the iron ions in the resulting precipitate gradually dissolve. It
266 can be seen from Fig. S2 that the soluble iron ions in the solution mainly exist in the
267 form of Fe^{3+} , and the concentration of Fe^{2+} in the solution was below $0.2 \text{ mg}\cdot\text{L}^{-1}$
268 throughout the reaction.

269

270 **3.1.2 Applied voltage**

271 To fix the iron powder on the $\text{RuO}_2\text{-IrO}_2/\text{Ti}$ plate, we applied a magnetic field. At
272 first, the iron powder was uniformly coated in an area of 8 cm^2 and then stacked and
273 erected on the $\text{RuO}_2\text{-IrO}_2/\text{Ti}$ plate with a needle shape after the magnetic field was
274 applied. Therefore, the area occupied by the iron powder was less than 8 cm^2 , but the
275 surface area of the entire $\text{mZVI-RuO}_2\text{-IrO}_2/\text{Ti}$ anode increased. Accurate calculation
276 of the surface area and current density of the $\text{mZVI-RuO}_2\text{-IrO}_2/\text{Ti}$ anode was difficult;

277 thus, this experiment was performed in a constant voltage mode. Different constant
278 voltages of 4, 6, 8, and 10 V were applied in the experiments to investigate their
279 influence on ammonia and phosphate removal. With the application of increasing
280 voltage from 4 V to 10 V, the ammonia removal efficiency increased from 33.61% to
281 98.95% (Fig. 2b). As the voltage increased, the ammonia removal rate simultaneously
282 increased. The increase in voltage caused the current and the electron transfer rate on
283 the electrode to increase, thereby promoting the formation of active intermediates (Cl_2 ,
284 HClO , and ClO^-) that have strong oxidizing properties and increase the rate of
285 ammonia oxidation. At a voltage of 10 V, the phosphate can be completely removed
286 within 15 min only, whereas that at 4 V was within 90 min (Fig. 2e). As the voltage
287 was increased from 4 V to 10 V, the dissolution rate of iron powder on the anode
288 increased. The rate at which $\text{Fe}^{2+}/\text{Fe}^{3+}$ and phosphate reacted to form precipitates also
289 increased. Ammonia removal rate was considerably lower than the phosphate removal
290 rate (Figs. 2b and 2e). The voltage should not be excessively low during simultaneous
291 ammonia and phosphate removal; otherwise, it would result in lower ammonia
292 removal efficiency.

293

294 **3.1.3 Initial pH**

295 In our electrical system, initial pH exerted considerably less significant influence
296 on ammonia removal compared with either anode materials or voltage. Fig. 2c shows
297 that pH increased as the ammonia removal rate increased. Under acidic conditions

298 (pH from 3 to 7), the removal rate of ammonia increased gradually, but such rate was
299 relatively fast under alkaline conditions (pH from 7 to 11). Furthermore, under acidic
300 conditions, the Cl_2 produced by the anode was more likely to escape and cause Cl_2
301 loss. However, an increased pH condition was more conducive to
302 chloride–chlorine–hypochlorite–chloride cycle, thereby increasing the amount of free
303 Cl_2 produced in the solution and accelerating ammonia degradation (Chen et al.
304 2007).

305 Fig. 2f illustrates the effect of initial pH from 3 to 11 on the phosphate
306 concentration remaining in the solution. Phosphate can be completely removed at pH
307 values of 3, 5, and 7. At pH 9, the phosphate removal rate slightly decreased but could
308 achieve 97.42% of the removal rate within 4 h. However, such rate was only 37.53%
309 at pH 11. Thus, $\text{Fe}(\text{OH})_3$ was easily formed when the OH^- concentration in the
310 solution was high, and the solubility of FePO_4 increased under strong alkaline
311 conditions (Irdemez et al. 2006). When the initial pH of the solution was 3 to 7, the
312 final pH dropped to approximately 2–3 after 4 h of electrolysis (Fig. 3b). The initial
313 pH was 9, and the final pH was reduced to 6.22 after the reaction. The pH of the
314 strong alkaline solution did not change substantially before and after the reaction
315 (initial pH=11 and final pH=11.15). Chen et al. found that the final pH decreased
316 when ammonia was removed by $\text{RuO}_2\text{-IrO}_2\text{-TiO}_2/\text{Ti}$ electrodes (Chen et al. 2007).
317 This finding could be due to the fact that pH is influenced by both cathodic and
318 anodic processes, as well as by the reactions of chlorine in water. The pH gradually

319 decreased as the electrolysis progressed because the Cl_2 generated by Cl^- electrolysis
320 was dissolved in water, and reactions (3) and (4) occurred to gradually lower the pH.
321 In the electrolyte where Cl^- and NH_4^+ coexist, the ammonia was oxidized by free
322 chlorine, and the reaction is shown in Eq. (5). The ammonia oxidation reaction
323 produced hydrochloric acid, and the pH of the solution gradually decreased as the
324 electrolytic oxidation reaction proceeded. Lacasa et al. found that the final pH
325 increased when phosphate was removed by iron anodes (Lacasa et al. 2011). As
326 shown in Eq. (10), the cathode consumed hydrogen ions under acidic and neutral
327 conditions to produce hydrogen, or generated hydroxide ions under alkaline
328 conditions, causing the pH in the solution to rise. Thus, the pH change caused by the
329 oxidation of ammonia plays a major role in the EO/EC process.

330

331 ***3.1.4 Zero-valent iron dosage***

332 Zero-valent iron dosage is an important part of the composite electrode. The
333 amount of iron powder may dramatically affect the removal of ammonia and
334 phosphate. As depicted in Fig. 4a, when the zero-valent iron dosage was increased
335 from 0.1 g to 0.4 g, the degradation rate of ammonia gradually decreased. Hence, the
336 more the amount of iron powder on the anode surface, the more electrons were
337 needed to convert zero-valent iron into iron ions so that the rate at which Cl^- loses
338 electrons at the anode will decrease. The area of the $\text{RuO}_2\text{-IrO}_2/\text{Ti}$ plate occupied by a
339 greater amount of iron powder was larger than any other areas because the latter was
340 more densely erected on the $\text{RuO}_2\text{-IrO}_2/\text{Ti}$ plate after being adsorbed by the magnet.

341 Consequently, a smaller area was generated for the RuO₂-IrO₂/Ti plate to provide
342 electron transfer to Cl⁻. With increasing zero-valent iron dosage, the phosphate
343 removal rate also increased (Fig. 4c), indicating that the higher the concentration of
344 iron ions in the solution, the easier it is to form iron phosphate precipitate. However,
345 increasing the amount of iron powder in the EO/EC process is not necessary because
346 the phosphate can be completely removed within 30 min (the zero-valent iron dosage
347 was from 0.1 g to 0.4 g), whereas the complete degradation of ammonia took longer.
348 Hence, 0.1 g of iron powder could completely remove the phosphate in the solution,
349 as revealed by experimental results.

350

351 **3.1.5 Reaction temperature**

352 Figs. 4b and 4e illustrate the removal of ammonia and phosphate at different
353 temperatures. As the temperature increased, the removal rates of ammonia and
354 phosphate also increased. Ammonia was completely removed within 4 h when the
355 reaction temperature was 25 °C. Moreover, ammonia could be completely removed
356 within 2 h when the temperature was 55 °C. For phosphate removal, the removal rate
357 was extremely fast at each temperature. This phenomenon can be explained by the
358 fact that the ionic strength and conductivity in the solution increased as the
359 temperature increased, thereby accelerating the rate of electron transfer. Ammonia
360 degradation was consistent with pseudo-zero order kinetics. Ammonia concentration
361 decreased linearly with time at all three different temperatures (25, 35, 45, and 55 °C)
362 in the electrochemical oxidation process (Fig. 5b). The slopes of lines were -0.96,

363 -1.10, -1.51, and -1.72 with correlation coefficients of 0.998, 0.983, 0.996, and 0.997,
364 respectively. Correspondingly, the ammonia oxidation rates were 0.96, 1.10, 1.51, and
365 1.72 mg N L⁻¹ min⁻¹ (Fig. 5b).

366

367 **3.1.6 Organic compounds**

368 Organic compounds may coexist in water with ammonia and phosphate in practical
369 applications. Wastewater discharged from various industries, such as coke plants,
370 pharmaceuticals, textiles, distilleries, and wineries, always contains organic pollutants
371 at high concentrations (Hu et al. 2019, Pan et al. 2018). In order to investigate the
372 effect of organic compounds on simultaneous ammonia and phosphate removal,
373 different concentrations of isopropanol (0, 10, 25, 50mM·L⁻¹) were added to the
374 previously solution. Fig. 4c reveals the influence of organic compounds on the
375 ammonia removal by the mZVI-RuO₂-IrO₂/Ti anode at 25 °C in a pH 7 aqueous
376 solution. The ammonia degradation rate was the fastest without organic compounds in
377 the solution. When the concentration of isopropanol was increased from 0 to 25
378 mM·L⁻¹, the degradation rate of ammonia gradually decreased. This indicated when
379 organic compounds coexist in the solution with ammonia and phosphate, the
380 intermediate oxidant oxidizes part of the organic compounds in addition to the
381 oxidation of ammonia. Continue to increase the concentration of isopropanol in the
382 solution to 50 mM·L⁻¹, the rate of ammonia degradation was almost unchanged.
383 Moreover, ammonia could be almost completely removed within 4 hours, regardless

384 of whether the system contains organic compounds. Conversely, the presence of
385 organic compounds has no effect on phosphate removal and phosphate can be
386 removed extremely quickly, regardless of the concentration of isopropanol (Fig. 4f).

387 In addition, we investigated the effect of magnetic field strength on simultaneous
388 removal of ammonia and phosphate. From Fig S3 we find that the strength of the
389 magnetic field in our system has no effect on the removal of ammonia and phosphate.
390 Therefore, the magnet is only used to attract iron powder in this system. Compared to
391 other single EO or EC processes, this electrochemical system was designed to achieve
392 simultaneous ammonia and phosphate removal by using the mZVI-RuO₂-IrO₂/Ti
393 anode (Table S1).

394

395 ***3.2 Characterization of precipitation***

396 The crystallinity and structure of the samples were evaluated via the XRD
397 technique. The XRD patterns of the precipitate obtained via reaction at different pH
398 values are shown in Fig. 6. The vacuum-dried samples were essentially amorphous
399 with no distinct characteristic peaks (Fig. 6a). To increase the crystallinity of the
400 precipitate, we calcined the precipitate in a nitrogen atmosphere for 2 h (set and
401 maintained at 600 °C for 2 h and then cooled to room temperature). The composition
402 of the precipitate varied at different pH values (Fig. 6b). When the initial pH was 3,
403 no apparent characteristic peak before calcination was observed, but a single broad
404 peak appeared from 20° to 35° after calcination. This broad peak is likely to indicate

405 iron oxides, but this requires further analysis due to the amorphous nature of iron
406 oxides, which are not easily detected by XRD (Yoon et al. 2016). As the pH value
407 rose to 5, some peaks appeared from 20° to 35°; but the peak intensity was extremely
408 low. When the initial pH of the solution was 7, the characteristic peaks of $\text{Fe}_2(\text{PO}_4)_\text{O}$
409 (PDF #85-2384) and Fe_2O_3 (PDF #73-2234) appeared (Fig. 6c). The appearance of
410 iron oxide indicated that the precipitate contained $\text{Fe}(\text{OH})_3$, which decomposed at a
411 high temperature of 600 °C to form Fe_2O_3 . When the initial pH of the solution was 9
412 and 11, the characteristic peaks of $\text{Fe}_2(\text{PO}_4)_\text{O}$ disappeared; when the pH increased, the
413 intensity of the peak also increased, while the line width decreased, indicating an
414 increase in crystallinity. Only the characteristic peak of Fe_2O_3 (PDF #73-2234)
415 appeared when the initial pH was 11 (Fig. 6d). This finding confirmed that under
416 higher pH conditions, $\text{Fe}(\text{OH})_3$ was more likely to be formed, resulting in an
417 undesirable effect of phosphate removal. This result is consistent with the conclusions
418 we have previously obtained (Fig. 2f).

419 Given the different phosphate removal effects at various pH conditions, we
420 investigated the morphology and elemental composition of the precipitate at pH 5 and
421 11, respectively. The morphologies of the precipitates obtained at the initial pH of 5
422 and 11 are shown in Figs. 7a and 7c. SEM results indicated that the precipitates were
423 loose, without a noticeable regular shape. The elemental mapping images of the
424 precipitate with a selected area (Figs. 7b and 7d) reveal that it contained Fe, P, and O
425 after the EO/EC process. The atomic percentage of P was 7.6% and 2.8% in the initial

426 pH of 5 and 11, respectively (Table 1). The density of P on the precipitate obtained at
427 pH 5 was higher than that on the precipitate obtained at pH 11. The atomic
428 concentration ratio of P in the precipitate obtained at pH 5 and 11 was approximately
429 0.37. This result is consistent with the previously obtained phosphate removal rate of
430 only 37.53% at pH of 11.

431 XPS was used to identify the chemical states of Fe, P, and O in the flocs produced
432 during the EO/EC process. The binding energy was calibrated to adventitious carbon
433 C 1s peak centered at 284.6 eV (Sleiman et al. 2016), and peak fittings were
434 performed using the XPSPeak41 software. To determine the valence of iron and the
435 form of P in the precipitate after the reaction, differentiating fitting of Fe 2p, O 1s, and
436 P 2p was performed. In addition to Fe, P, and O, the precipitate also contained a small
437 amount of S element (Fig. 8a). Considering that nitrogen-containing wastewater was
438 configured using $(\text{NH}_4)_2\text{SO}_4$, flocs may adsorb trace amounts of sulfate in the solution.
439 Fig. 8b shows the high-resolution XPS spectrum of Fe $2p_{3/2}$, which can be
440 deconvoluted into two peaks at 709.7 and 712.6 eV, corresponding to the ferric
441 divalent iron and trivalent iron, respectively (Bae and Lee 2014, Chen et al. 2018).
442 The high-resolution XPS spectrum of the O 1s (Fig. 8c) could be fitted into three
443 peaks at binding energies of 529.9, 531.3, and 532.1 eV, which corresponded to the
444 lattice oxygen in the metal oxide (O^{2-}), the hydroxide in the surface hydroxyls (OH^-),
445 and the chemically or physically adsorbed water ($\text{H}_2\text{O}_{\text{ads}}$) (Chen et al. 2018, Tan et al.
446 2018). Therefore, iron hydroxide and iron oxide were formed after the reaction. The P

447 2p XPS spectrum of precipitation was deconvoluted into two peaks of 132.9 and
448 133.7 eV, which corresponded to PO_4^{3-} and HPO_4^{2-} , respectively (Fig. 8d) (Yin and
449 Kong 2014). Thus, PO_4^{3-} and HPO_4^{2-} groups existed on the surface of the precipitation
450 after the reaction.

451 **3.3 Energy consumption**

452 Energy consumption is an essential aspect of electrochemical processes, and large
453 energy consumption is an important reason for restricting electrochemical methods.
454 Table 2 shows the energy consumption during the EO/EC process at 10 V. As the
455 reaction progressed, the energy consumption increased. When the reaction was
456 performed for 180 min and the ammonia removal rate reached 98.84%, the energy
457 consumption for ammonia removal was $0.622 \text{ kWh}\cdot\text{g}^{-1} \text{ N}$. Meanwhile, phosphate can
458 be completely removed by the reaction in only 30 min, and the energy consumption
459 for phosphate removal was $0.216 \text{ kWh}\cdot\text{g}^{-1} \text{ P}$. In this experiment, the energy
460 consumption was mainly determined by the energy consumed by the ammonia
461 removal process. Methods for further reducing energy consumption are one of the
462 issues to be studied in the future.

463 **4. Conclusions**

464 The mZVI-RuO₂-IrO₂/Ti electrode was designed and successfully combined with
465 the EO/EC process to simultaneously remove ammonia and phosphate. Results of this
466 study revealed that mZVI-RuO₂-IrO₂/Ti electrode is extremely effective in removing
467 ammonia and phosphate. Increasing the voltage and temperature also demonstrated

468 positive effects. The rate of ammonia removal increased slightly with increasing
469 initial pH. Conversely, phosphate was poorly removed under alkaline conditions.
470 Therefore, simultaneous removal of ammonia and phosphate was suitably
471 demonstrated at a neutral pH. In addition, zero-valent iron dosage had a minimal
472 effect on the removal of ammonia but significantly enhanced phosphate removal by
473 addition of iron powder. Ammonia could be completely removed within 180 min at
474 the applied voltage of 10 V, pH of 7, zero-valent iron dosage of 0.1 g, and reaction
475 temperature of 35 °C using mZVI-RuO₂-IrO₂/Ti anode. The phosphate removal rate
476 was extremely fast and could be completely removed within 30 min under the same
477 conditions. This work reports the excellent performance of the mZVI-RuO₂-IrO₂/Ti
478 electrode in removing ammonia and phosphate. Hence, future studies should use
479 mZVI-RuO₂-IrO₂/Ti electrode to treat actual wastewater.

480

481 **Acknowledgments**

482 Financial support for this work was provided by Natural Science Foundation of
483 Zhejiang Province (Y18E080055).

484

485

486

487

488

489

490 **References**

- 491 Bae, S. and Lee, W. (2014) Influence of riboflavin on nanoscale zero-valent iron
492 reactivity during the degradation of carbon tetrachloride. *Environ Sci Technol* 48(4),
493 2368-2376.
- 494 Bashir, M.J.K., Aziz, H.A., Yusoff, M.S. and Adlan, M.N. (2010) Application of
495 response surface methodology (RSM) for optimization of ammoniacal nitrogen
496 removal from semi-aerobic landfill leachate using ion exchange resin. *Desalination*
497 254, 154-161.
- 498 Bassin, J.P., Kleerebezem, R., Dezotti, M. and van Loosdrecht, M.C. (2012)
499 Simultaneous nitrogen and phosphate removal in aerobic granular sludge reactors
500 operated at different temperatures. *Water Res* 46(12), 3805-3816.
- 501 Bektas, N., Akbulut, H., Inan, H. and Dimoglo, A. (2004) Removal of phosphate from
502 aqueous solutions by electro-coagulation. *J Hazard Mater* 106(2-3), 101-105.
- 503 Bonmati, A. and Flotats, X. (2003) Air stripping of ammonia from pig
504 slurry: characterization and feasibility as a pre- or post-treatment to mesophilic
505 anaerobic digestion. *Waste Manag* 23(3), 261-272.
- 506 Boujelben, N., Bouzid, J., Elouear, Z., Feki, M., Jamoussi, F. and Montiel, A. (2008)
507 Phosphorus removal from aqueous solution using iron coated natural and engineered
508 sorbents. *J Hazard Mater* 151(1), 103-110.
- 509 Chen, G.H. (2004) Electrochemical technologies in wastewater treatment. *Sep Purif*
510 *Technol* 38(1), 11-41.
- 511 Chen, J.L., Shi, H.C. and Lu, J.H. (2007) Electrochemical treatment of ammonia in
512 wastewater by RuO₂-IrO₂-TiO₂/Ti electrodes. *J Appl Electrochem* 37, 1137-1144.
- 513 Chen, W., Zhang, A., Gu, Z. and Li, Q. (2018) Enhanced degradation of refractory
514 organics in concentrated landfill leachate by Fe⁰/H₂O₂ coupled with microwave
515 irradiation. *Chemical Engineering Journal* 354, 680-691.
- 516 Choi, J.W., Lee, S.Y., Park, K.Y., Lee, K.B., Kim, D.J. and Lee, S.H. (2011)
517 Investigation of phosphorous removal from wastewater through ion exchange of

- 518 mesostructure based on inorganic material. *Desalination* 166(1-3), 281-285.
- 519 Cossu, R., Polcaro, A., Lavagnolo, M., Mascia, M., Palmas, S. and Renoldi, F. (1998)
- 520 Electrochemical treatment of landfill leachate oxidation at Ti/PbO₂ and Ti/SnO₂.
- 521 *Environ Sci Technol* 32, 3570-3573.
- 522 Costa, C.R., Botta, C.M., Espindola, E.L. and Olivi, P. (2008) Electrochemical
- 523 treatment of tannery wastewater using DSA electrodes. *J Hazard Mater* 153(1-2),
- 524 616-627.
- 525 Fan, N., Li, Z., Zhao, L., Wu, N. and Zhou, T. (2013) Electrochemical denitrification
- 526 and kinetics study using Ti/IrO₂-TiO₂-RuO₂ as the anode and Cu/Zn as the cathode.
- 527 *Chemical Engineering Journal* 214, 83-90.
- 528 Fernandes, A., Pacheco, M.J., Ciríaco, L. and Lopes, A. (2015) Review on the
- 529 electrochemical processes for the treatment of sanitary landfill leachates: Present and
- 530 future. *Appl Catal B:Environ* 176-177, 183-200.
- 531 Gendel, Y. and Lahav, O. (2012) Revealing the mechanism of indirect ammonia
- 532 electrooxidation. *Electrochim Acta* 63, 209-219.
- 533 Heidmann, I. and Calmano, W. (2008) Removal of Zn(II), Cu(II), Ni(II), Ag(I) and
- 534 Cr(VI) present in aqueous solutions by aluminium electrocoagulation. *J Hazard Mater*
- 535 152(3), 934-941.
- 536 Hu, Q., Zhou, N., Gong, K., Liu, H., Liu, Q., Sun, D., Wang, Q., Shao, Q., Liu, H.,
- 537 Qiu, B. and Guo, Z. (2019) Intracellular Polymer Substances Induced Conductive
- 538 Polyaniline for Improved Methane Production from Anaerobic Wastewater Treatment.
- 539 *ACS Sustainable Chemistry & Engineering* 7(6), 5912-5920.
- 540 Huang, H., Xiao, D., Pang, R., Han, C. and Ding, L. (2014) Simultaneous removal of
- 541 nutrients from simulated swine wastewater by adsorption of modified zeolite
- 542 combined with struvite crystallization. *Chemical Engineering Journal* 256, 431-438.
- 543 Huang, H., Xiao, X., Yan, B. and Yang, L. (2010) Ammonium removal from aqueous
- 544 solutions by using natural Chinese (Chende) zeolite as adsorbent. *J Hazard Mater*
- 545 175(1-3), 247-252.

- 546 Ihara, I., Umetsu, K., Kanamura, K. and Watanabe, T. (2006) Electrochemical
547 oxidation of the effluent from anaerobic digestion of dairy manure. *Bioresour Technol*
548 97(12), 1360-1364.
- 549 Irdemez, S., Demircioglu, N. and Yildiz, Y.S. (2006) The effects of pH on phosphate
550 removal from wastewater by electrocoagulation with iron plate electrodes. *J Hazard*
551 *Mater* 137(2), 1231-1235.
- 552 Jaffer, Y., Clark, T.A., Pearce, P. and Parsons, S.A. (2002) Potential phosphorus
553 recovery by struvite formation. *Water Res* 36(7), 1834-1842.
- 554 Jih, C.G., Huang, J.S. and Hsieh, K.C. (2001) Performance evaluation of single-sludge
555 reactor system treating high-strength nitrogen wastewater. *J Hazard Mater* B85,
556 213-227.
- 557 Kapałka, A., Joss, L., Anglada, Á., Comninellis, C. and Udert, K.M. (2010a) Direct
558 and mediated electrochemical oxidation of ammonia on boron-doped diamond
559 electrode. *Electrochem Commun* 12(12), 1714-1717.
- 560 Kapałka, A., Katsaounis, A., Michels, N.L., Leonidova, A., Souentie, S., Comninellis,
561 C., Udert, K.M. and more, S. (2010b) Ammonia oxidation to nitrogen mediated by
562 electrogenerated active chlorine on Ti/PtOx-IrO₂. *Electrochem Commun* 12(9),
563 1203-1205.
- 564 Lacasa, E., Cañizares, P., Sáez, C., Fernández, F.J. and Rodrigo, M.A. (2011)
565 Electrochemical phosphates removal using iron and aluminium electrodes. *Chem Eng*
566 *J* 172, 137-143.
- 567 Laurenzi, M., Falas, P., Robin, O., Wick, A., Weissbrodt, D.G., Nielsen, J.L., Ternes,
568 T.A., Morgenroth, E. and Joss, A. (2016) Mainstream partial nitrification and anammox:
569 long-term process stability and effluent quality at low temperatures. *Water Res* 101,
570 628-639.
- 571 Li, L. and Liu, Y. (2009) Ammonia removal in electrochemical oxidation: mechanism
572 and pseudo-kinetics. *J Hazard Mater* 161(2-3), 1010-1016.
- 573 Li, X., Wang, C., Qian, Y., Wang, Y. and Zhang, L. (2013) Simultaneous removal of

- 574 chemical oxygen demand, turbidity and hardness from biologically treated citric acid
575 wastewater by electrochemical oxidation for reuse. *Separation and Purification*
576 *Technology* 107, 281-288.
- 577 Lin, L., Yuan, S., Chen, J., Xu, Z. and Lu, X. (2009) Removal of ammonia nitrogen in
578 wastewater by microwave radiation. *J Hazard Mater* 161(2-3), 1063-1068.
- 579 Ma, J., He, C., He, D., Zhang, C. and Waite, T.D. (2018) Analysis of capacitive and
580 electro-dialytic contributions to water desalination by flow-electrode CDI. *Water Res*
581 144, 296-303.
- 582 Omwene, P.I., Koby, M. and Can, O.T. (2018) Phosphorus removal from domestic
583 wastewater in electrocoagulation reactor using aluminium and iron plate hybrid
584 anodes. *Ecological Engineering* 123, 65-73.
- 585 Pan, D., Ge, S., Zhao, J., Shao, Q., Guo, L., Zhang, X., Lin, J., Xu, G. and Guo, Z.
586 (2018) Synthesis, characterization and photocatalytic activity of mixed-metal oxides
587 derived from NiCoFe ternary layered double hydroxides. *Dalton Trans* 47(29),
588 9765-9778.
- 589 Pressley, T.A., Bishop, D.F. and Roan, S.G. (1972) Ammonia-nitrogen removal by
590 breakpoint chlorination. *Environ Sci Technol* 6(7), 622-628.
- 591 Profeti, D., Lassali, T.A.F. and Olivi, P. (2006) Preparation of $\text{Ir}_{0.3}\text{Sn}_{(0.7-x)}\text{Ti}_x\text{O}_2$
592 electrodes by the polymeric precursor method: Characterization and lifetime study. *J*
593 *Appl Electrochem* 36(8), 883-888.
- 594 Ruiz, G., Jeison, D., Rubilar, O., Ciudad, G. and Chamy, R. (2006)
595 Nitrification-denitrification via nitrite accumulation for nitrogen removal from
596 wastewaters. *Bioresour Technol* 97(2), 330-335.
- 597 Sleiman, N., Deluchat, V., Wazne, M., Mallet, M., Courtin-Nomade, A., Kazpard, V.
598 and Baudu, M. (2016) Phosphate removal from aqueous solution using ZVI/sand bed
599 reactor: Behavior and mechanism. *Water Res* 99, 56-65.
- 600 Smith, V.H. and Schindler, D.W. (2009) Eutrophication science: where do we go from
601 here? *Trends Ecol Evol* 24(4), 201-207.

- 602 Su, Y., Cui, H., Li, Q., Gao, S. and Shang, J.K. (2013) Strong adsorption of phosphate
603 by amorphous zirconium oxide nanoparticles. *Water Res* 47(14), 5018-5026.
- 604 Tan, C., Dong, Y., Fu, D., Gao, N., Ma, J. and Liu, X. (2018) Chloramphenicol
605 removal by zero valent iron activated peroxymonosulfate system: Kinetics and
606 mechanism of radical generation. *Chemical Engineering Journal* 334, 1006-1015.
- 607 Tian, Y.S., He, W.H., Liang, D.D., Yang, W.L., Logan, B.E. and Ren, N.Q. (2018)
608 Effective phosphate removal for advanced water treatment using low energy,
609 migration electric-field assisted electrocoagulation. *Water Res* 138, 129-136.
- 610 Xue, W.-J., Cui, Y.-H., Liu, Z.-Q., Yang, S.-Q., Li, J.-Y. and Guo, X.-L. (2020)
611 Treatment of landfill leachate nanofiltration concentrate after ultrafiltration by
612 electrochemically assisted heat activation of peroxydisulfate. *Separation and*
613 *Purification Technology* 231.
- 614 Yin, H. and Kong, M. (2014) Simultaneous removal of ammonium and phosphate
615 from eutrophic waters using natural calcium-rich attapulgite-based versatile
616 adsorbent. *Desalination* 351, 128-137.
- 617 Yoon, I.H., Yoo, G., Hong, H.J., Kim, J., Kim, M.G., Choi, W.K. and Yang, J.W.
618 (2016) Kinetic study for phenol degradation by ZVI-assisted Fenton reaction and
619 related iron corrosion investigated by X-ray absorption spectroscopy. *Chemosphere*
620 145, 409-415.
- 621 Zhang, C., He, D., Ma, J. and Waite, T.D. (2018a) Active chlorine mediated ammonia
622 oxidation revisited: Reaction mechanism, kinetic modelling and implications. *Water*
623 *Res* 145, 220-230.
- 624 Zhang, X., Lin, H.J. and Hu, B. (2018b) The effects of electrocoagulation on
625 phosphorus removal and particle settling capability in swine manure. *Sep Purif*
626 *Technol* 200, 112-119.
- 627 Zheng, X.Y., Kong, H.N., Wu, D.Y., Wang, C., Li, Y. and Ye, H.R. (2009) Phosphate
628 removal from source separated urine by electrocoagulation using iron plate electrodes.
629 *Water Sci Technol* 60(11), 2929-2938.

630 Zhu, X., Ni, J. and Lai, P. (2009) Advanced treatment of biologically pretreated
631 coking wastewater by electrochemical oxidation using boron-doped diamond
632 electrodes. Water Res 43(17), 4347-4355.

633

Journal Pre-proof

Table 1 Surface elemental composition and atomic percentages via EDS analysis for the precipitate obtained at pH 5 and 11.

Initial pH	Element (atomic %)		
	O	Fe	P
5	65.40	27.00	7.60
11	62.80	34.40	2.80

Table 2 Energy consumption and removal efficiency of ammonia and phosphate at different reaction times.

reaction time (min)		5	15	30	60	120	180
N	Energy consumption (kWh·g ⁻¹ N)	0.358	0.463	0.529	0.506	0.511	0.622
	Removal efficiency (%)	4.70	11.66	20.33	43.39	85.98	98.84
P	Energy consumption (kWh·g ⁻¹ P)	0.059	0.109	0.216	0.430	0.853	1.272
	Removal efficiency (%)	61.60	99.78	100.00	100.00	100.00	100.00

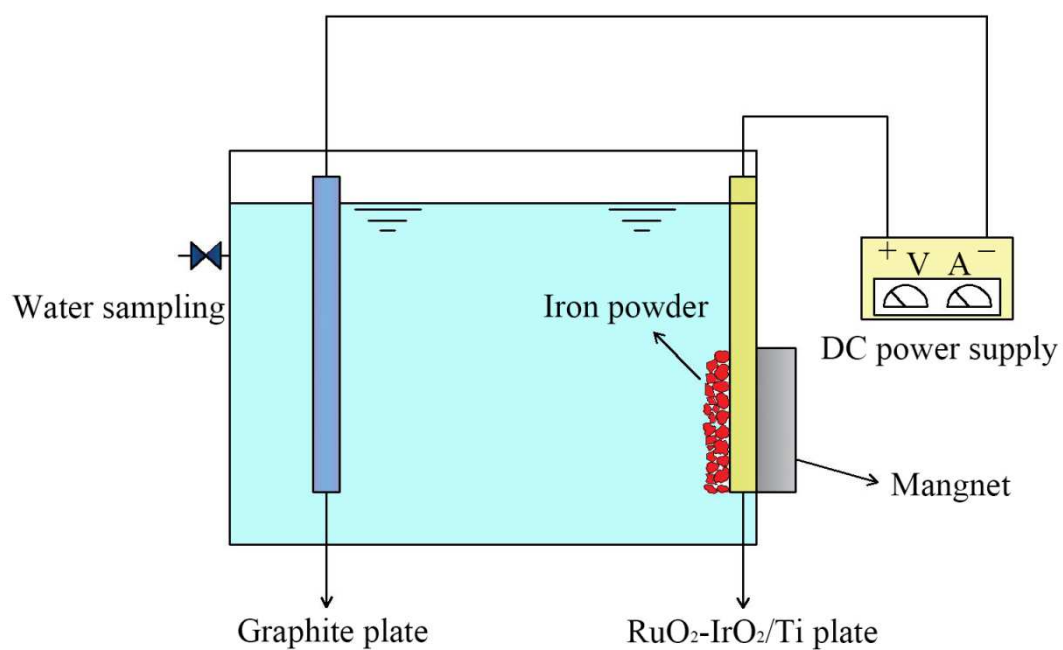


Figure 1 Schematic diagram of the experimental setup.

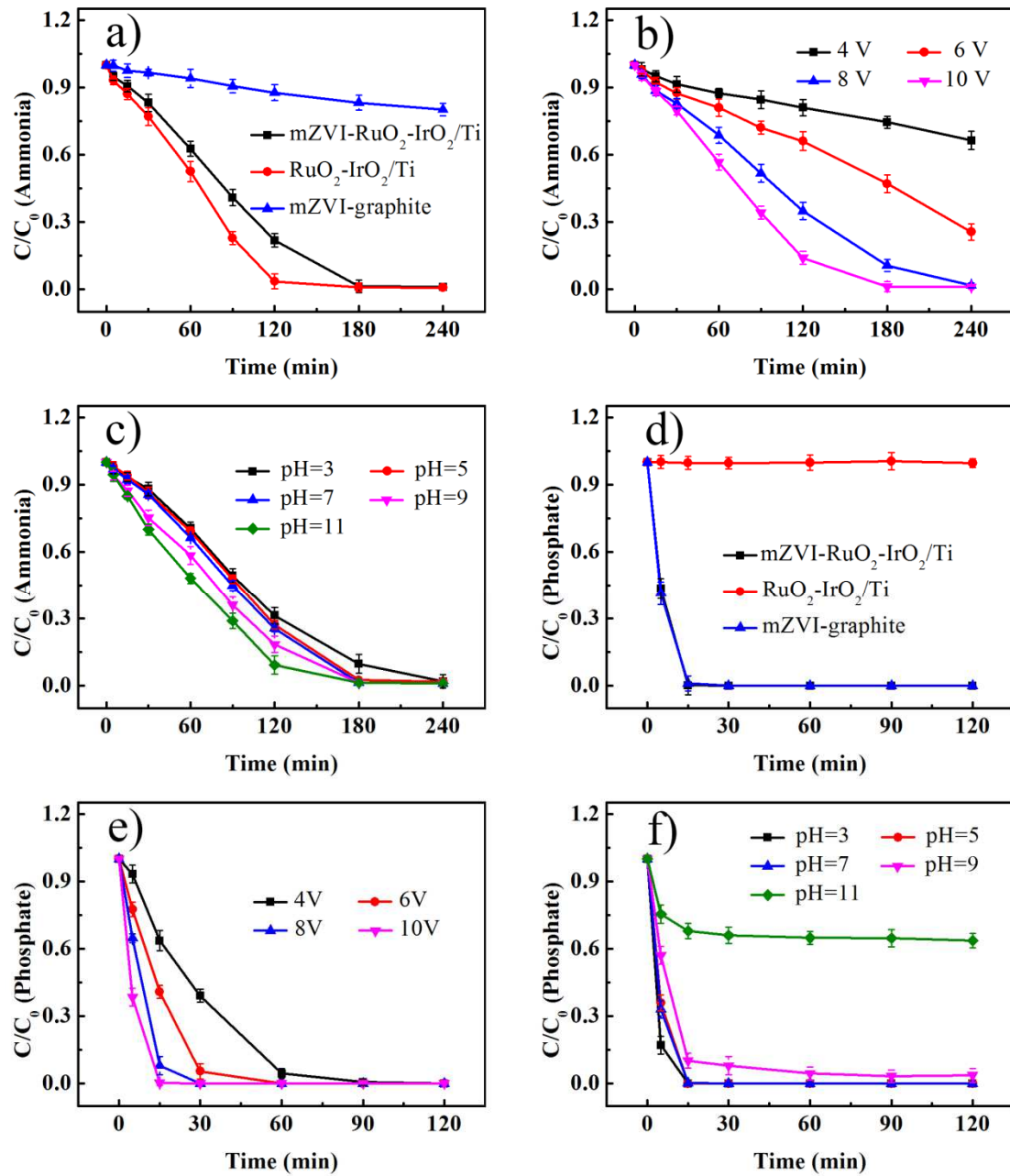


Figure 2 Influence of different factors on ammonia removal: a) anode materials, b) voltage, and c) initial pH; and influence of different factors for phosphate removal: d) anode materials, e) voltage, and f) initial pH.

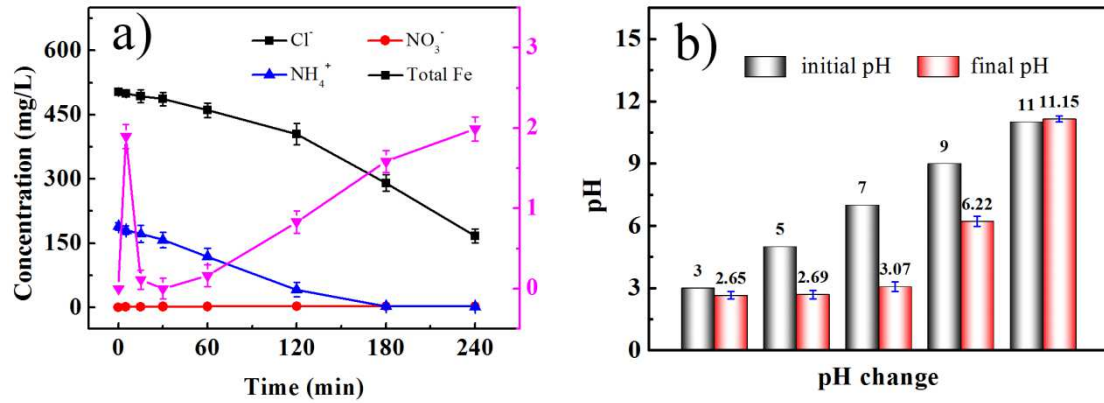


Figure 3 a) Concentrations of Cl⁻, NH₄⁺, NO₃⁻, and total soluble iron ions in solution changes with time; b) pH change at different initial pH values.

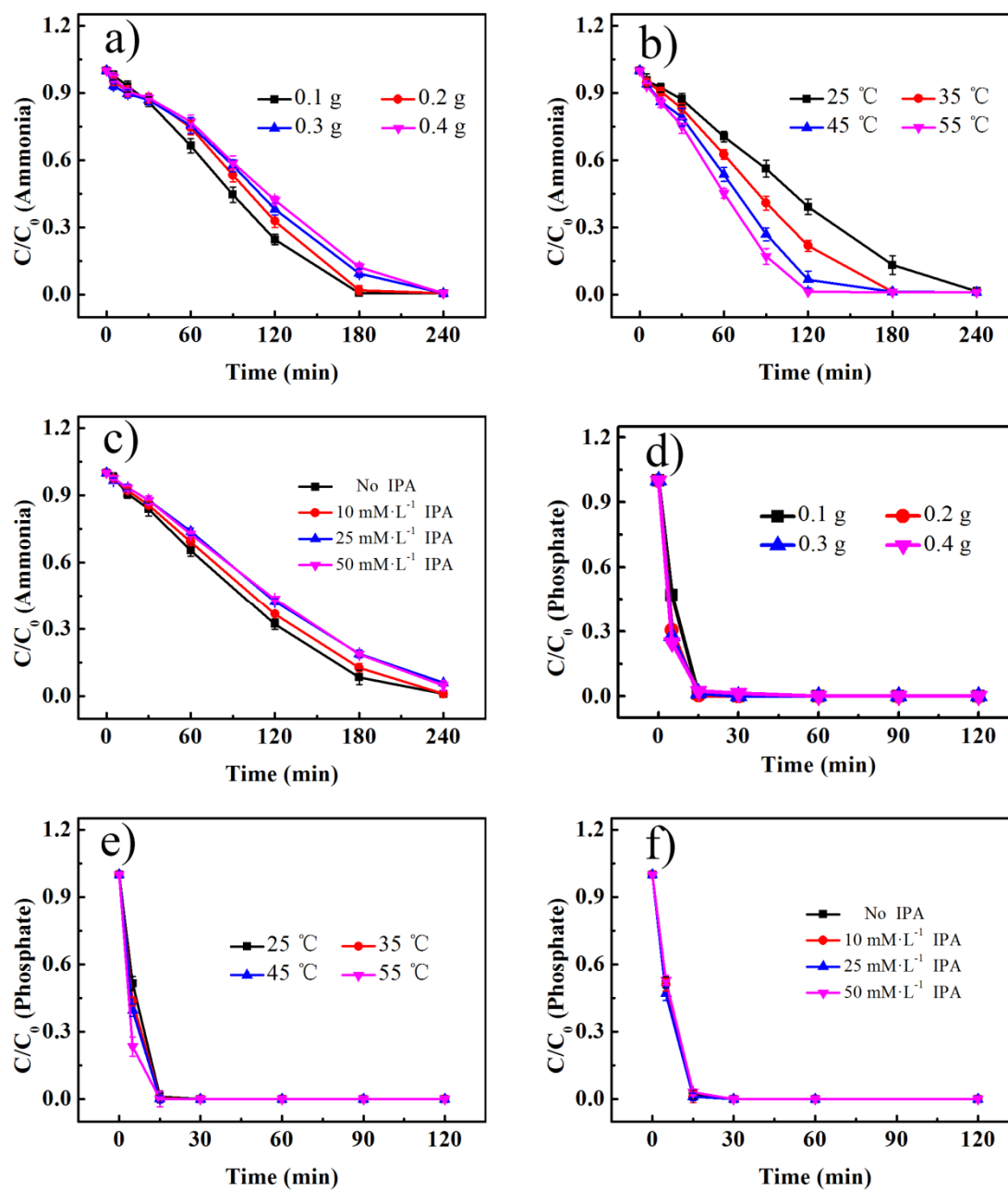


Figure 4 Influence of different factors on ammonia removal: a) zero-valent dosage, b) reaction temperature, c) organic compounds; and influence of different factors on phosphate removal: d) zero-valent iron dosage, e) reaction temperature, f) organic compounds.

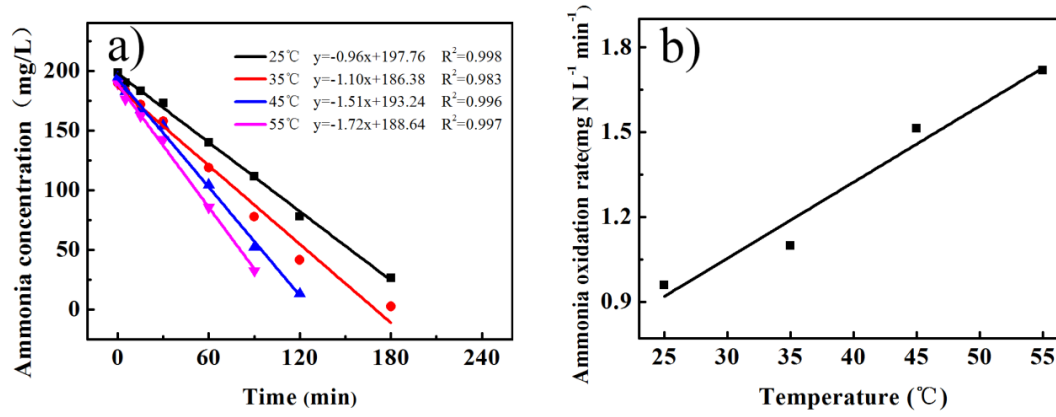


Figure 5 Effect of different reaction temperatures on a) ammonia concentration profiles and b) ammonia oxidation rate.

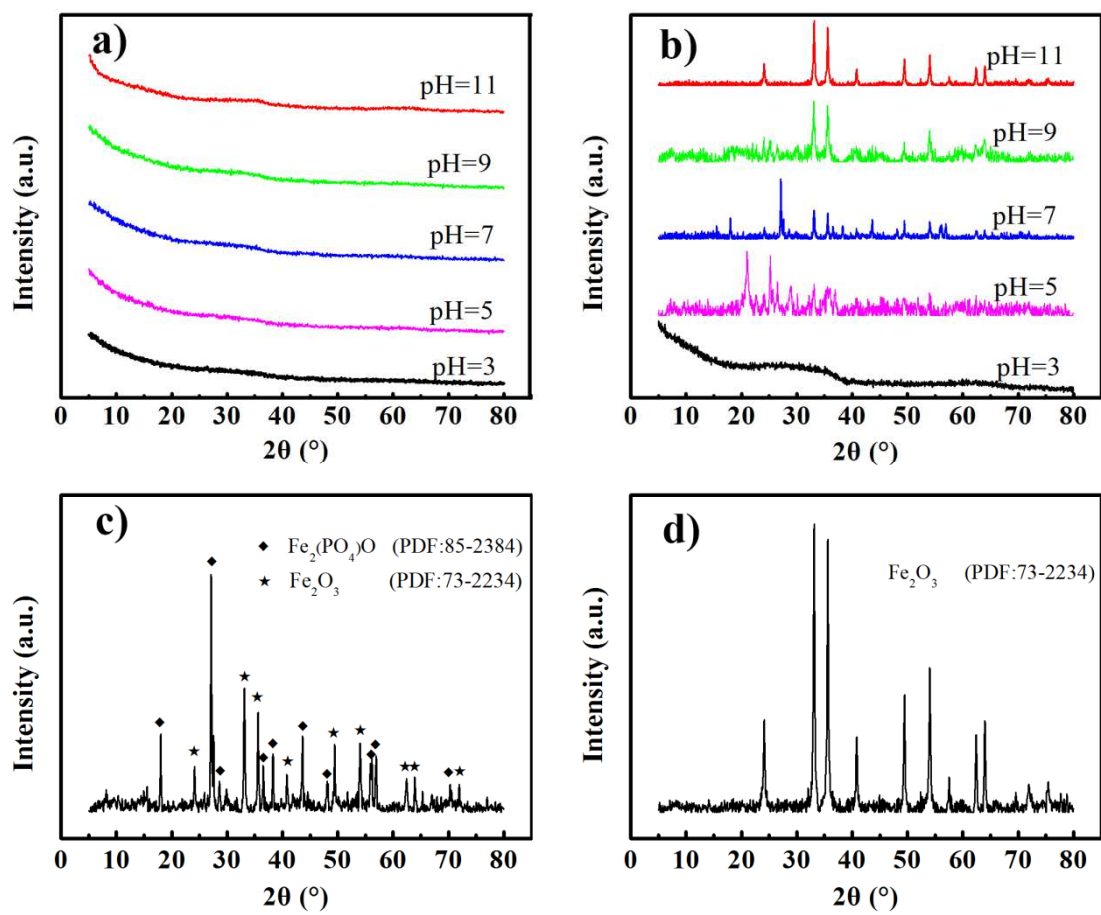


Figure 6 XRD patterns at different pH values: a) after vacuum drying; b) calcination at 600 °C; c) calcination at 600 °C, pH=7; and d) calcination at 600 °C, pH=11.

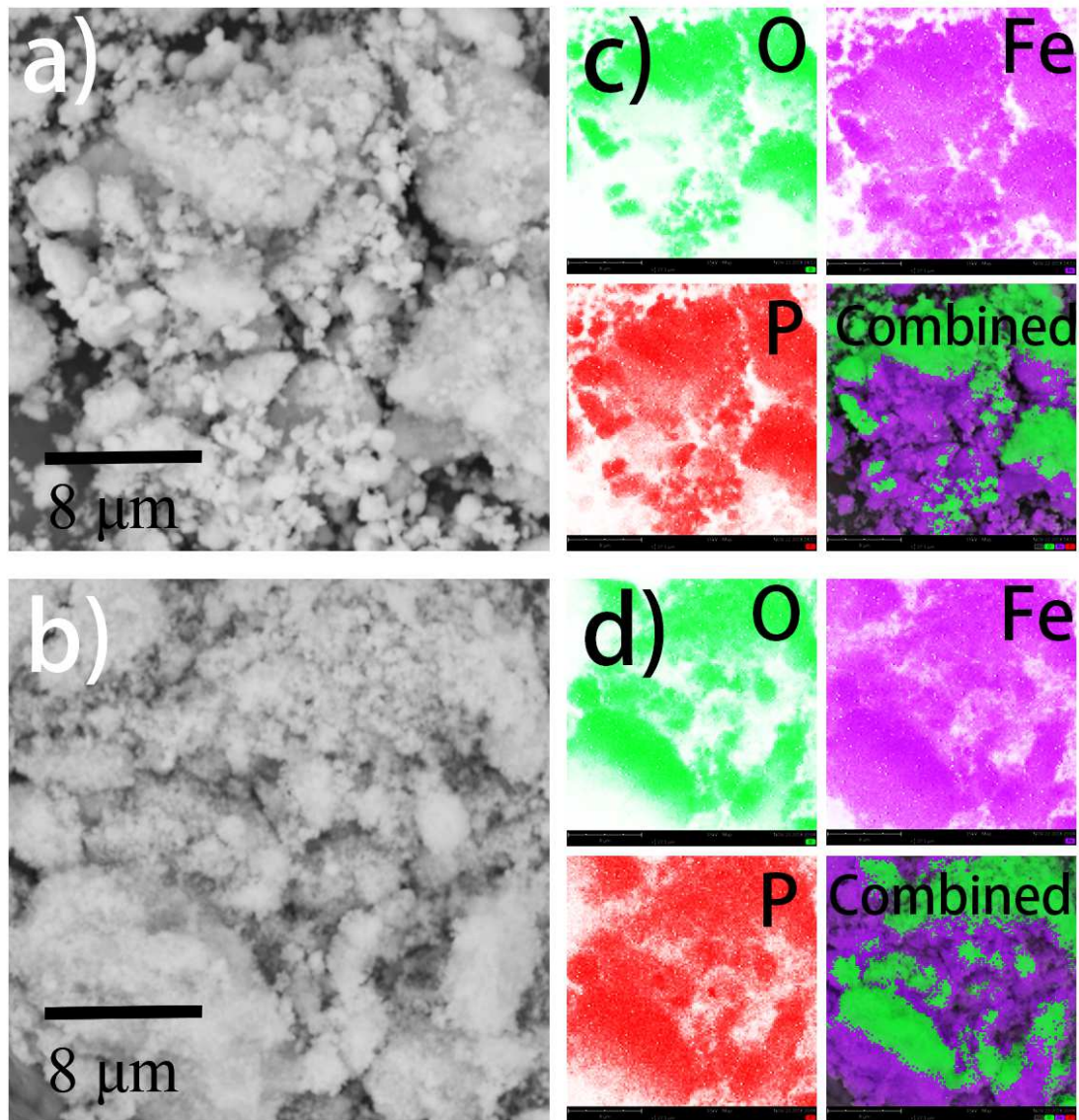


Figure 7 SEM image of precipitation at a) pH=5 and b) pH=11, and elemental mapping of precipitation at c) pH=5 and d) pH=11.

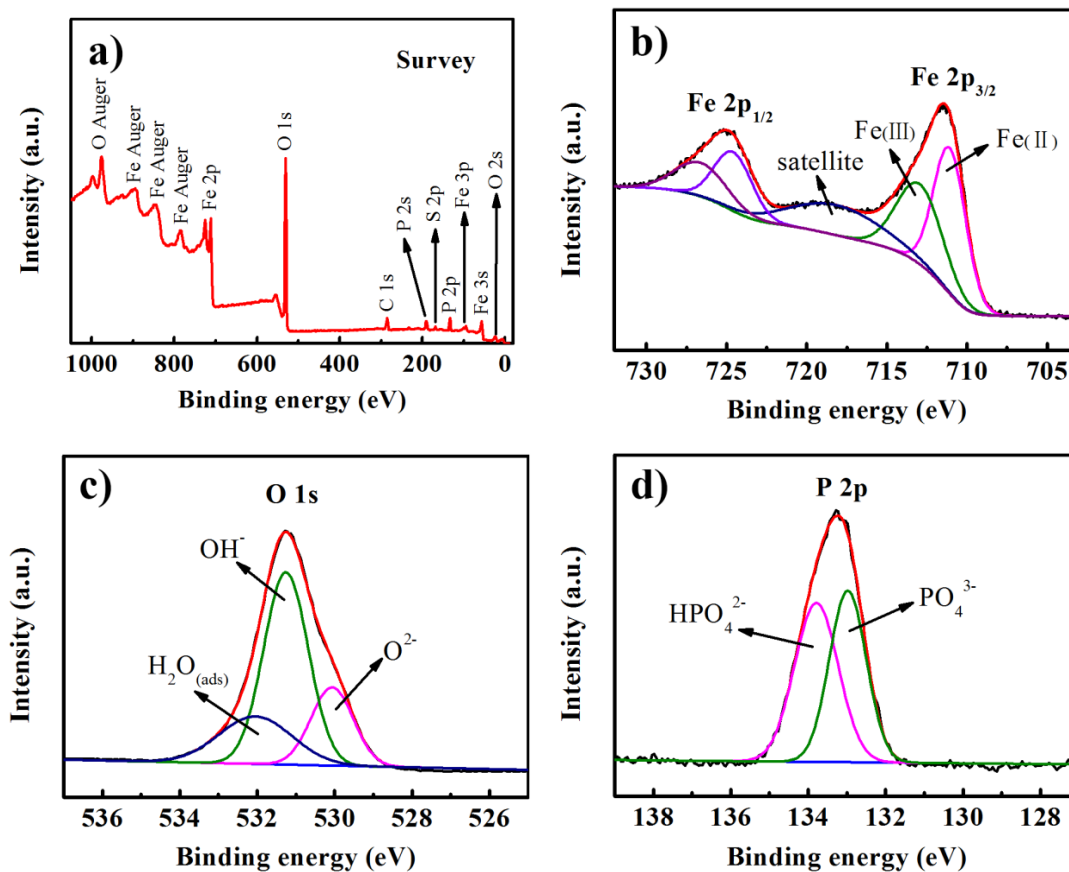


Figure 8 XPS spectra of the surface elements of the precipitation: a) survey spectrum, b) Fe element, c) O element, and d) P element of the precipitation.

Highlights:

- ▶ RuO₂-IrO₂/Ti plate combined with iron powder act as an anode of electrochemical unit.
- ▶ Iron powder were immobilized at the surface of the RuO₂-IrO₂/Ti plate by a magnet.
- ▶ The mZVI-RuO₂-IrO₂/Ti anode showed high simultaneous removal efficiency of N and P.
- ▶ N and P were synergistically removed by electro-oxidation and electrocoagulation.

Declaration of Interest Statement

We declare that we do not have any commercial or associative interest that represents a conflict of interest in connection with the work submitted

Journal Pre-proof